Overcharging of DNA in the Presence of Salt: Theory and Simulation

Markus Deserno,[†,‡] Felipe Jiménez-Ángeles,[§,¶] Christian Holm,[†] and Marcelo Lozada-Cassou*[,§,¶]

Max-Planck-Institut für Polymerforschung, Ackermannweg 10, 55128 Mainz, Germany, Department of Chemistry and Biochemistry, UCLA, 405 Hilgard Avenue, Los Angeles, California 90095, Departamento de Física, Universidad Autónoma Metropolitana-Iztapalapa, Apartado Postal 55-534, 09340 México D.F., México, and Programa de Simulación Molecular, Instituto Mexicano del Petróleo, Lázaro Cárdenas 152, 07730 México, D. F., México

Received: March 7, 2001; In Final Form: June 29, 2001

A study of a model rodlike polyelectrolyte molecule immersed in a monovalent or divalent electrolyte is presented. Results for the local concentration profile, mean electrostatic potential, charge distribution function, and ζ-potential are obtained from hypernetted-chain/mean spherical approximation (HNC/MSA) theory and compared with molecular dynamics (MD) simulations. As a particular case, the parameters of the polyelectrolyte molecule are mapped to those of a DNA molecule. Both HNC/MSA and MD predict the occurrence of overcharging, which is not present in the Poisson−Boltzmann theory. Further an excellent qualitative, and in some cases quantitative, agreement between HNC/MSA and MD is found. Oscillations observed in the mean electrostatic potential, local concentration profiles, and the curvature of the ζ-potential are discussed in terms of the observed overcharging effect. Particularly interesting results are a very nonmonotonic behavior of the ζ-potential, as a function of the rod charge density, and the overcharging by *monovalent* counterions.

I. Introduction

"Polyelectrolytes are polymers bearing ionizable groups, which, in polar solvents, can dissociate into charged polymer chains (macroions) and small counterions".[1] The combination of macromolecular properties and long-range electrostatic interactions results in an impressive variety of phenomena. It makes these systems interesting from a fundamental as well as a technological point of view. A thorough understanding of polyelectrolytes has become increasingly important in biochemistry and molecular biology. This is because virtually all proteins, as well as the DNA, are polyelectrolytes. Their interactions with each other and with the charged cell membrane are still far from being fully understood, which is partly because of the intricate coupling between ion distribution and chain conformation.

A first approach to the problem is to fix the conformation of the chain and to focus on a detailed description of the counterion distribution. Usually polyelectrolytes stretch because of the electrostatic repulsion of their charged groups. Moreover, many important polyelectrolytes have a large intrinsic stiffness (e.g., DNA, actin filaments, or microtubules). Therefore, a rodlike conformation is an obvious first choice. The remaining problem of charged rods immersed in solution is much easier, but is still far from being exactly solvable.

An additional approximation, which is frequently used in theoretical descriptions, is to completely integrate out the counterionic degrees of freedom. On a linearized mean-field level this yields a Debye−Hückel-like theory characterized by a screened Coulomb potential between charged monomers. To obtain the correct physical properties, one uses an *effective* Yukawa potential, which in turn requires adjustable parameters such as an effective polyelectrolyte radius and charge. In this way the dependence of the ionic structure, hereafter called electrical double layer (EDL), around two or more polyelectrolytes, as a function of the polyelectrolyte−polyelectrolyte distance, is not accounted for. This information, however, is most relevant for the understanding of polyelectrolyte aggregation or self-assembling. This effect is more important for polyelectrolytes in low-concentration added salt solution, because the ionic screening is weak for this case. This has been relevant for charged plates and charged spherical macroions.[2−4]

A common further approximation assumes that the investigation of a small subvolume containing only one rod and its counterions will suffice to unveil much of the interesting physics. The main justification for this approach is that the subvolume has zero net charge. Moreover, the counterions will also efficiently screen higher order multipoles. Hence, the interactions between two such subvolumes, which are neglected when focusing on just one rod, will be fairly weak. This approximation is called cylindrical cell model, and it provides the framework for our simulation calculation.

One attractive feature of the cell model is that in the salt-free case the nonlinear Poisson−Boltzmann (PB) equation can be solved *exactly* in this geometry.[5,6] It also clearly displays the effect of partial counterion *condensation*.[7,8] Although a charged sphere loses all its counterions upon dilution, a charged plane keeps all of them. For a charged cylinder the fraction of ions, which upon dilution remain in the vicinity of the macroion, can be anywhere between 0 and 100%. Addition of salt increases the screening of the charged rod. If the salt content is large enough, the electric field will have decayed to zero before the

[†] Max-Planck-Institut für Polymerforschung.
[‡] UCLA.
[§] Universidad Autónoma Metropolitana-Iztapalapa.
[¶] Instituto Mexicano del Petróleo.

10.1021/jp010861+ CCC: $20.00 © 2001 American Chemical Society
Published on Web 10/11/2001

cell radius is reached. It is then permissible to extend the latter to infinity. This is the approach that we use for our integral equation calculations.

The PB theory has limitations for systems in which ion correlations become important.[9] It cannot predict the attractive forces that are seen experimentally in DNA solutions[10] and that have also been found in various simulation[11−13] and integral equation[14−16] studies in the presence of multivalent counterions.

In this article we present studies for a rod immersed in a salt solution which PB theory fails to describe correctly, namely, the possibility of overcharging a single rod, resulting in an effective charge reversal, and the appearance of a nonmonotonic ζ-potential.[17−19] This effect is most relevant in electrophoresis experiments.[20] The overcharging of a macroion modifies in a nonlinear fashion the electrophoretic mobility as a function of the polyelectrolyte charge and salt concentration. This effect is not included in the classical electrophoresis theory of Wiersema et al.[21] and O'Brien and White,[22] which is a linear theory based on the PB description of the EDL around the polyelectrolyte.

The EDL obtained through the well-established integral equation approach does predict overcharging.[17,18] The overcharging effect has been observed in Monte Carlo (MC) simulations for planar,[23] cylindrical,[24] and spherical[25,26] geometries. Moreover, several years ago, Gonzales-Tovar et al.[18] predicted that for some macroion charges and electrolyte concentrations the overcharging produces an electrophoresis mobility reversal. This mobility reversal has been observed experimentally.[27−30] This effect has been taken into account in the electrophoresis theory by Lozada-Cassou et al.[31] An excellent qualitative agreement with experimental results[20,28,30] is found. This overcharging effect and the predicted mobility reversal have been addressed recently by Deserno et al.[9] and Shklovskii and colleagues.[32,33]

In ref 9 ion distributions are studied via the integrated charge distribution function, $P(r)$, and overcharging is addressed based on molecular dynamics (MD) simulations. In this article we extend this research by approaching the overcharging effect through a well-established integral equation theory[17,18] as well as more detailed MD simulations. We compute $P(r)$, the concentration profiles $g_i(r)$, the mean electrostatic potential profile $\psi(r)$, and the ζ-potential. A comparison of the integral equation results with those from MD is presented.

II. Simulational Details of the Model System

A. Generating a Cell Geometry. Compared with the spherical cell model, the cylindrical model presents one additional but crucial complication: the charged rod is infinitely long. Several methods have been proposed in the literature to handle this problem. They essentially all use a hexagonal prism with a certain height as a unit cell. This approximates the cylindrical cell by the "most round" space-filling object. In this publication we take a computationally even simpler approach by using a *cubic* unit box of side-length L_b and placing the DNA parallel to one of the edges (see Figure 1). The justification for this approach is as follows. In a high-salt environment the charged rod will be screened within a distance much smaller than the size of the box. The potential will therefore become constant long before the deviations from a cylindrical cell will be felt. It is thus largely irrelevant, whether these deviations are of the hexagonal or cubic type. When comparing with the cylindrical cell model, a radius $R = L_b/\sqrt{\pi}$ is appropriate, because it yields the same area per rod.

The main advantage of this approach is that such a system can be treated with the plain cubic Ewald sum or one of its mesh upgrades.[34−37] This permits a very efficient way to compute the long-range electrostatic interactions.

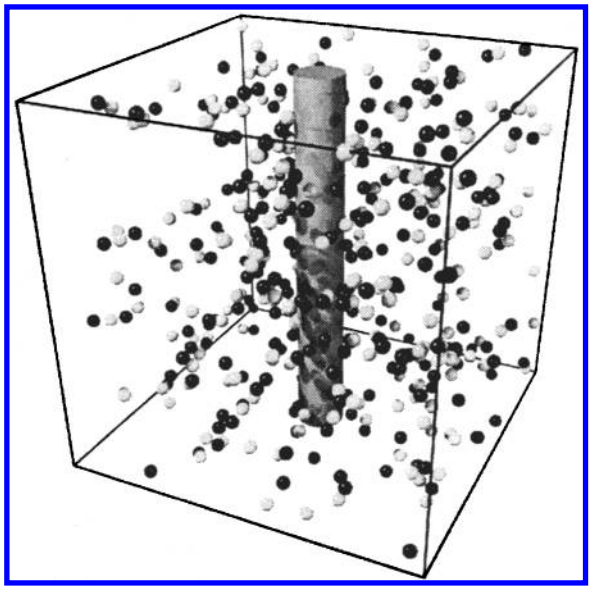

Figure 1. Realization of the cell model. A rod of length L_b placed parallel to an edge of a cube of side length L_b yields an infinite square array of infinitely long rods upon periodic replication of the cubic box. The dark particles are the counterions or positive salt ions, and the bright particles are the negative salt ions. This particular snapshot contains 36 divalent counterions, 220 positive and 220 negative divalent salt ions.

B. Interaction Potentials and DNA Mapping. A specification of two interaction potentials is necessary to describe the model system: (*i*) an excluded volume interaction preventing two particles from occupying the same position in space and (*ii*) the long-range Coulomb potential.

For the excluded volume interaction between the ions we use the following potential:

$$V^*_{\text{ion-ion}}(r) = \begin{cases} 4\epsilon\left[\left(\frac{a}{r}\right)^{12} - \left(\frac{a}{r}\right)^{6} + \frac{1}{4}\right] & 0 < r \le r_{\text{cut}} \equiv 2^{1/6}a \\ 0 & r_{\text{cut}} < r \end{cases} \quad (1)$$

Without the cutoff this would be the common Lennard−Jones potential describing particles with a diameter a and an attractive potential minimum of ϵ. To achieve pure repulsion, we cut the potential at the minimum and shift it up such that it smoothly goes to zero there. As a consequence, ϵ becomes largely irrelevant. Because two ions that are a distance a apart have the (repulsive) interaction energy ϵ, we make the natural choice $\epsilon = k_B T$.

To give the rod a larger radius than the ions, we use an ion-rod potential similar to eq 1, in which r is replaced by $r - r_s$. This shifts the hard core a distance r_s toward larger radii and gives a distance of closest approach of $r_s + a$. Because the ions have diameter a, this corresponds to a rod radius r_0 of $r_0 = r_s + a/2$. Of course, in this case, r is a cylindrical and not a spherical radial coordinate.

The electrostatic interaction energy between two ions with charge $z_i e_0$ and $z_j e_0$, is given by

$$V^{\text{el}}_{ij}(r) = k_B T \frac{z_i z_j l_B}{r} \quad \text{with} \quad l_B = \frac{{e_0}^2}{4\pi\epsilon_0\epsilon_r k_B T} \quad (2)$$

where z_i is the valence of the i species and e_0 is the elemental

TABLE 1: System Parameters for the DNA Simulations

parameter	symbol	value	value in LJ units
ion diameter	a	4.25 Å	a
ion valence	z	2	2
rod radius	r_0	7.86 Å	1.85 a
line charge density (DNA)	λ	$-e_0$/1.7 Å	$-2.5\ e_0/a$
Bjerrum length (water)	l_B	7.14 Å	1.68 a
Manning parameter	ξ	4.2	4.2
box size	L_b	122.4 Å	28.8 a
corresponding cell radius	R	69.1 Å	16.2 a
temperature	T	298 K	ϵ/k_B

charge. By definition the Bjerrum length l_B is the distance at which two unit charges have interaction energy k_BT. With the vacuum dielectric constant $\epsilon_0 = 8.85 \times 10^{-12}$ C^2 m^{-2} N^{-1} and the dielectric coefficient $\epsilon_r = 78.5$ applying to water at room temperature, one gets a Bjerrum length of approximately 7.14 Å. The line charge density λ of the rod is modeled by placing unit charges along the rod axis at the distance $b = e_0/\lambda$. The number of charges along the rod per Bjerrum length is an important dimensionless measure of the line charge density and is often referred to as the Manning parameter.

$$\xi = \frac{\lambda l_B}{e_0} = \frac{l_B}{b} \tag{3}$$

Its relevance lies in the fact that for $\xi > 1$ the phenomenon of counterion "condensation" is observed.[7]

Within the periodic boundary conditions used during the simulations, the presence of such long-range interactions poses both mathematical and technical difficulties. We use an efficient fast Fourier transform accelerated Ewald sum, the P^{3}M algorithm, which scales almost linearly with the number of charges.[35−37]

The final step consists of explicitly mapping the parameters to a DNA system in aqueous solution. This affects ion diameter a, rod radius r_0, Bjerrum length l_B, and line charge density λ. Our choice is presented in Table 1.We performed MD simulations of the rod systems by using a Langevin thermostat to drive the system into the canonical state.[38] The real-space and Fourier-space part of the electrostatic energy was used to check for equilibration. The observables presented originate from averaging more than roughly 1500 independent configurations.

III. Hypernetted-Chain/Mean Spherical Approximation Theory

The integral equation formalism is a well-established statistical mechanical approach that has been reliable when it is applied to simple microscopic models of inhomogeneous fluids.[39,40] A particularly successful integral equation theory for inhomogeneous, charged fluids is the so-called hypernetted-chain/mean spherical approximation (HNC/MSA).[25,41−43] The HNC/MSA theory for a model charged rod, immersed in an electrolyte, has been derived previously.[17,18] In this article, we solve the HNC/MSA equation for an infinitely long, hard, charged cylinder of radius r_0, with uniform line charge density λ. The rod is immersed in a two-component restricted primitive model electrolyte (RPM), i.e., a fluid of charged hard spheres of diameter a with a centered point charge z_ie_0.

The fluid electroneutrality condition is

$$\sum_{m=1}^{2} z_m\rho_m = 0 \tag{4}$$

where ρ_m is the bulk concentration of species m. To satisfy the necessary condition of zero electrical field at infinity, the rod charge is compensated by the charge induced in the fluid, λ':

$$\lambda' \equiv 2\pi \int_{r_0+a/2}^{\infty} \rho_{el}(r) r\, dr = -\lambda, \quad \text{with}$$

$$\rho_{el}(r) \equiv e_0 \sum_{m=1}^{2} z_m\rho_m(r) \tag{5}$$

The local concentration profile of the species m is denoted as $\rho_m(r)$. The solvent is taken as a dielectric continuum of dielectric constant ϵ_r. For simplicity, rod and solvent are assumed to have the same dielectric constant, to avoid complications with dielectric boundaries.

It has long been recognized in physics that particles and fields are equivalent in the sense that both are defined through their interaction potentials. This simple fact has been applied in the past to derive, in a straightforward manner, inhomogeneous integral equation theories from the Ornstein−Zernike (OZ) equation for homogeneous fluids.[40,44] The homogeneous three-component OZ equation is

$$h_{ij}(\mathbf{r}_{21}) = c_{ij}(\mathbf{r}_{21}) + \sum_{m=1}^{3} \rho_m \int h_{im}(\mathbf{r}_{23}) c_{mj}(\mathbf{r}_{13}) d\nu_3 \tag{6}$$

where $h_{ij}(\mathbf{r}_{21})$ and $c_{ij}(\mathbf{r}_{21})$ are the total and direct correlation functions, between particle 2 located at $\mathbf{r}_2$ and particle 1 at $\mathbf{r}_1$ of species i and j, respectively, $\mathbf{r}_{21} \equiv \mathbf{r}_2 - \mathbf{r}_1$.

Consequently, one can consider a particle of a fluid as a source of an external field or an external field as a particle of the fluid. Applying this simple idea to eq 6, one can think of one of the species, say α, as made of infinite cylindrical rods and the remaining two species as ions. In α's infinite dilution limit the cylinders are uncorrelated. Hence, letting $\rho_\alpha \to 0$, the OZ equation for an ionic solution next to a charged cylinder reads

$$h_{\alpha j}(\mathbf{r}_{21}) = c_{\alpha j}(\mathbf{r}_{21}) + \sum_{m=1}^{2} \rho_m \int h_{\alpha m}(\mathbf{r}_{23}) c_{mj}(\mathbf{r}_{13}) d\nu_3 \tag{7}$$

In the past, several approximations (or "closures") for the direct correlation function have been suggested. Two of them are:

$$\ln[g_{ij}(\mathbf{r}_{21})] = -\beta V_{ij}(\mathbf{r}_{21}) + h_{ij}(\mathbf{r}_{21}) - c_{ij}(\mathbf{r}_{21}) \tag{8}$$

$$c_{ij}(\mathbf{r}_{21}) = -\beta V_{ij}(\mathbf{r}_{21}) \tag{9}$$

Equations 8 and 9 are known as the HNC equation and the MSA, respectively; $V_{ij}(\mathbf{r}_{21})$ is the direct interaction potential between species i and j, and $\beta \equiv 1/k_BT$.

If the HNC closure is used for the direct correlation function between the rod particle and the j species, eq 7 becomes

$$g_{\alpha j}(\mathbf{r}_{21}) = \exp[-\beta V_{\alpha j}(\mathbf{r}_{21}) + \sum_{m=1}^{2} \rho_m \int h_{\alpha m}(\mathbf{r}_{23}) c_{mj}(\mathbf{r}_{13}) d\nu_3] \tag{10}$$

In this scheme, the two-particle correlation functions $h_{\alpha j}(\mathbf{r}_{21})$ and $c_{\alpha j}(\mathbf{r}_{21})$ correspond to the one-particle total, and direct inhomogeneous correlation functions $h_j(\mathbf{r})$ and $c_j(\mathbf{r})$ for species j of a fluid under the influence of an external field produced by a rod particle. The local concentration for the j species is given by $\rho_j(\mathbf{r}) = \rho_j g_j(\mathbf{r})$, where $g_j(\mathbf{r}) = h_j(\mathbf{r}) + 1$ is called the reduced concentration profile. Therefore, the charge concentration profile

in eq 5 is given by

$$\rho_{el}(r) = \sum_{m=1}^{2} z_m e_0 \rho_m g_m(r) \tag{11}$$

For this model the direct interaction potential between the rod and the j species of the fluid, $V_j(r)$, can be separated into two parts: the hard-sphere−hard-rod term $V_j^*(r)$ and the electrostatic interaction potential $V_j^{el}(r)$. The first takes into account the fact that ions cannot penetrate or deform the cylinder

$$V_j^* = \begin{cases} \infty & 0 < r \le r_0 + a/2 \\ 0 & r > r_0 + a/2 \end{cases} \tag{12}$$

The second can be found from Gauss' law and is given by

$$-\beta V_j^{el}(r) = 2 z_j \xi \ln(r) \; (r > r_0) \tag{13}$$

In the MSA closure the homogeneous direct correlation function for a RPM electrolyte has an analytical expression. This function can be written as

$$c_{mj}(s) = -\beta V_{mj}^{el}(s) + z_m z_j c_d^{sr}(s) + c_s^{hs}(s) \tag{14}$$

In the first term appears the direct electric interaction potential between the species of the fluid, which is given by eq 2, the second term is an electrical short-range function, and the third is the direct-correlation function for a hard-sphere fluid. When the MSA closure is used in the integral of eq 10, one obtains the HNC/MSA equation for an ionic fluid next to a charged rod. Taking advantage of the cylindrical geometry and the fact that the direct correlation function between the ions depends only on their relative distance $s \equiv |\mathbf{r}_1 - \mathbf{r}_3|$, eq 10 can be written as[17,18]

$$g_j(r) = \exp\{-\beta[z_j e_0 \psi(r) + J_j(r)]\} \tag{15}$$

where $\psi(r)$ is the mean electrostatic potential

$$-\beta e_0 \psi(r) = 2\xi \ln(r) + 2\pi l_B \int_{r_0+a/2}^{\infty} \rho_{cd}(y) \ln((r^2 + y^2 + |r^2 - y^2|)/2) y \mathrm{d}y \tag{16}$$

The $J_j(r)$ terms are integrals of the short-range terms of the direct correlation function

$$-\beta J_j(r) = z_j \int_{r_0+a/2}^{\infty} \rho_{cd}(y) L(r,y) \mathrm{d}y + \int_{r_0+a/2}^{\infty} \rho_{cs} K(r,y) \mathrm{d}y + \rho A(r) \tag{17}$$

with

$$\rho = \sum_{m=1}^{2} \rho_m$$

$$\rho_{cs}(y) = \sum_{m=1}^{2} \rho_m h_m(y)$$

$$\rho_{cd}(y) = \sum_{m=1}^{2} z_m \rho_m h_m(y)$$

and

$$L(r,y) = 4y \int_0^{\phi_{max}} \mathrm{d}\phi \int_0^{z_{max}} c_d^{sr}(s) \, \mathrm{d}z$$

$$K(r,y) = 4y \int_0^{\phi_{max}} \mathrm{d}\phi \int_0^{z_{max}} c_s^{hs}(s) \, \mathrm{d}z$$

$$A(r) = -\int_0^{r_0+a/2} K(r,y) \mathrm{d}y$$

where $s^2 = z^2 + r^2 + y^2 - 2ry \cos\phi$. In the limit $a \to 0$ of point ions, $c_d^{sr}(s)$ and $c_s^{hs}(s) \to 0$. Thus $J_j(r) \to 0$[17] and eq 15 becomes

$$g_m(r) = \exp[-\beta z_m e_0 \psi(r)] \tag{18}$$

where $\psi(r)$ is given by eq 16, which is the solution of the well-known PB differential equation for point ions around a charged cylindrical electrode, i.e.,

$$\frac{1}{r}\frac{\mathrm{d}\psi(r)}{\mathrm{d}r} + \frac{\mathrm{d}^2\psi(r)}{\mathrm{d}r^2} = -\frac{e_0}{\epsilon_0 \epsilon_r} \sum_{m=1}^{2} z_m \rho_m \exp[-\beta z_m e_0 \psi(r)] \tag{19}$$

Therefore, the integral equation version of the PB differential equation is[17]

$$g_j(r) = \exp\{2 z_j \xi \ln(r) + 2 z_j \pi_{-B} \int_{r_0+a/2}^{\infty} \rho_{cd}(y) \ln[(r^2 + y^2 + |r^2 - y^2|)/2] y \mathrm{d}y\} \tag{20}$$

which is also the HNC/MSA equation in the point ions limit. The differences between these two theories are due to the ionic size correlations that are partially taken into account in HNC/MSA theory but that are ignored in the PB equation. In the past, it has been shown that the size effects become important for strong field interaction, polyvalent ions and high salt concentration.[18]

The HNC/MSA and PB integral equations are solved numerically with efficient finite element methods.[16,45] The solution of eq 15 takes 1 min in a R12000 processor of an SGI machine. In our theoretical calculation we use the same input parameters as in our MD calculations. The salt concentration is obtained through

$$\rho_s = N_s / L_b^3 \tag{21}$$

where N_s is the number of salt molecules used in the simulation. Nevertheless, we have to point out the differences in the short-range interaction used in both models. Although in HNC/MSA we use hard particles, the MD (for technical reasons) uses the potential from eq 1, which has some surface softness. This results in an effective excluded volume, whose actual value depends on the interaction strength. At an interaction energy of $k_B T$ the particle diameter is a. However, if the particles attract each other strongly, they can come closer to each other.

IV. Results

We will discuss the results in terms of the mean electrostatic potential, $\psi(r)$, the local concentration profiles, $g_m(r)$, and the integrated charge distribution function

$$P(r) = \frac{1}{|\lambda|} \int_{r_0}^{r} \mathrm{d}\bar{r} \; 2\pi \bar{r} \rho_{el}(\bar{r}) \tag{22}$$

Figure 2 shows the HNC/MSA and MD results for $P(r)$ and $\psi(r)$, for five rod systems, for which the line charge density, and thereby the Manning parameter, has been successively increased. One system has a smaller Manning parameter than DNA and three have a larger. All systems have a Debye screening length, which is much smaller than the Manning radius

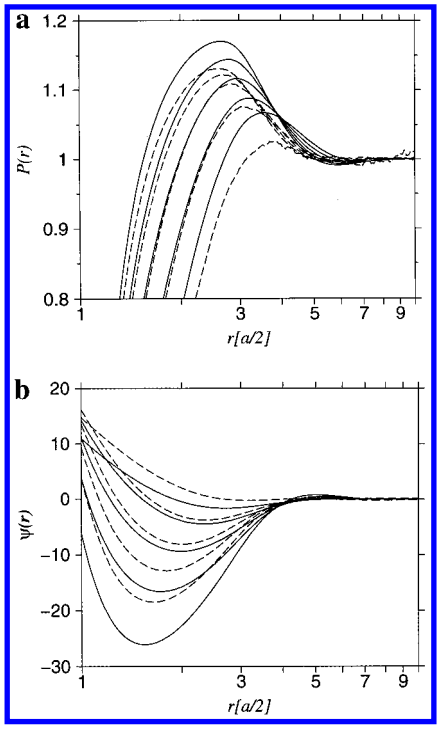

Figure 2. (a) Charge distribution function $P(r)$ and (b) mean electrostatic potential $\psi(r)$ for the parameters from Table 1. The electrolyte is a 0.49 M 2:2 salt. The distance r is measured with respect to the cylinder surface in units of the ionic radius. The solid and dashed lines correspond to the HNC/MSA and MD calculations, respectively. The different curves are for different values of the Manning parameter, $\xi = 2.1, 4.2, 6.3, 8.4, 10.5$, which correspond to surface charge densities of $\sigma = 0.095, 0.190, 0.286, 0.381, 0.476$ C/m^2, respectively. In $P(r)$, the surface charge density increases from bottom to top, whereas in the mean electrostatic potential it increases from top to bottom. The value $\xi = 4.2$ ($\sigma = 0.190$ C/m^2) corresponds to DNA.

of the corresponding salt-free system. According to the observations of ref 9 this means that the concept of Manning "condensation" is no longer meaningful. The rod charge is compensated by salt screening. According to simple PB theory, no remarkable features are to be expected in the bulk solution. Contrary to that, however, in Figure 2a $P(r)$ shows overcharging, i.e., the rod charge is over-compensated at a certain distance from the rod. For a given salt concentration the degree of overcharging is increased as the charge density increases. No overcharging saturation point is observed, at least for physical charge densities. Whereas in Figure 2a overcharging is present even for a very low charge density, such as $\sigma = 0.095$ C/m^2 our HNC/MSA calculations show overcharging for even lower rod charge densities. We will return to this point later. In Figure 2a, the maximum of overcharging is closer to the rod's suface as σ increases. This effect has implications for the location of the so-called ζ-potential in electrophoresis experiments.[31] As pointed out before,[18,23] overcharging implies a change of direction in the local electrical field. Our MD and HNC/MSA results are consistent with this fact, as shown in Figure 2b, where a minimum in $\psi(r)$ is observed. The value of r at the minimum of $\psi(r)$, i.e., where the electrical field is zero, concides with that at which $P(r) = 1$, as it should.

Integral equation theories give much more reliable results than the PB theory at high salt concentrations, polyvalent ions, and/or for fluids under the influence of strong external fields. This is because they partially take into account correlations due to the ionic size, which PB theory ignores. The HNC/MSA theory indeed correctly predicts the occurrence of overcharging, although it overestimates its amount. The qualitative agreement

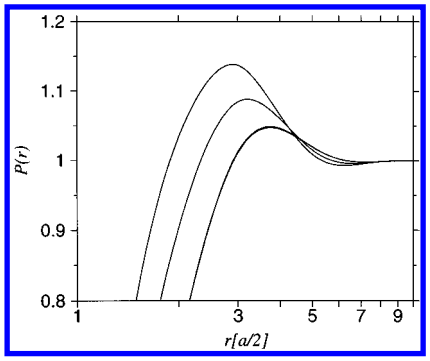

Figure 3. Charge distribution function from HNC/MSA for a RPM electrolyte next to a charged cylinder. The distance r is measured with respect to the cylinder surface in units of the ionic radius. The electrolyte is a 0.49 M 2:2 salt. The results correspond to different cylinder radii, whereas the Manning parameter has been held constant at $\xi = 4.2$. From top to bottom the cylinder radii are $r_0 = 3.86, 7.86, 110, 1200$ Å, which correspond to the surface charge densities $\sigma = 0.388, 0.190, 10^{-2}, 10^{-3}$ C/m^2, respectively. The curves for $r_0 = 110$ Å and $r_0 = 1200$ Å are indistinguishable on this scale.

between the HNC/MSA and MD results is excellent. The quantitative agreement is fair and particularly good for the DNA calculation. In the next section we will discuss the disagreement seen between the HNC/MSA and MD results for high and low cylinder charge densities.

For a given constant value of the Manning parameter, cylindrical macroions with different diameters will produce different EDL structures. In Figure 3, HNC/MSA results for rods with the same value of ξ but different diameters show different charge distributions $P(r)$. This illustrates the simple fact that the Manning parameter ξ alone is not sufficient to specify the ionic structure around cylindrical macroions. Because the ionic structure depends directly on the field strength, it is often better to use the cylinder's surface charge density σ, which is a direct measure of the electrical field that penetrates into the solution. Note, however, that ξ and σ are simply related by $\xi = 2\pi r_0 \sigma l_B/e_0$.

In Figure 4a and b we show HNC/MSA and MD reduced concentration profiles for $\sigma = 0.190$ C/m^2 ($\xi = 4.2$) and $\sigma = 0.49$ C/m^2 ($\xi = 10.5$), respectively, whereas all the other parameters are the same as in Figure 2. The value of r at the maximum of $P(r)$ matches with that where $g_+(r) = g_-(r)$, at least for symmetric electrolytes. Therefore the later oscillation in the local concentration profiles shows the attraction (repulsion) to coions (counterions) because of a change in direction of the effective electrical field. On the other hand, concentration profile oscillations are a consequence of the ionic size correlations. Hence, overcharging results from electrostatic attraction and size correlations.

The first maximum seen in the coion reduced concentration profile implies a coion concentration greater than its bulk value and indicates that the local electric field is attractive to coions. It is also observed that HNC/MSA overestimates the contact value of the distribution function with respect to MD predictions. The overestimation of HNC/MSA can be associated with two facts: *(i)* the excluded volume used in both models is different and *(ii)* HNC/MSA theory does not take into account all the size and charge correlations.

Another important phenomenon is indicated by the behavior of the mean electrostatic potential in Figure 2b. It concerns the value of this potential at the distance of closest approach between ions and the rod,

$$\zeta = \psi(r_0 + a/2) \tag{23}$$

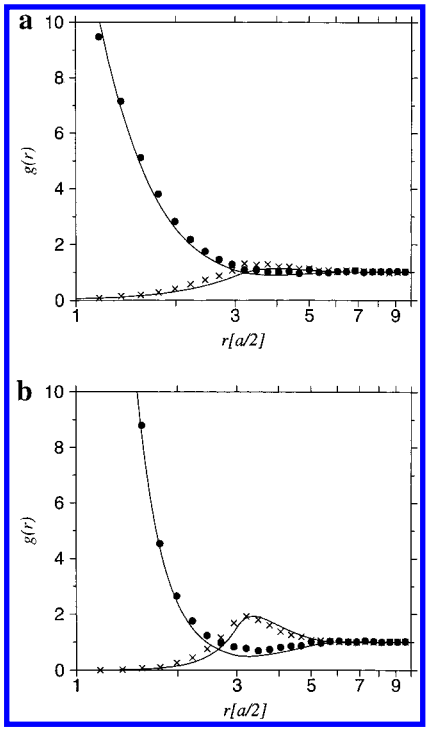

Figure 4. Reduced concentration profiles $g_i(r)$ for an electrolyte next to a charged cylinder. The electrolyte is a 0.49 M 2:2 salt. The distance r is measured with respect to the cylinder surface in units of the ionic radius. The system parameters are given in Table 1. (a) The results corresponding to $\xi = 4.2$ ($\sigma = 0.190$ C/m^2); (b) the results for $\xi = 10.5$ ($\sigma = 0.49$ C/m^2). The dots and crosses are the MD distribution functions for counterions and coions, respectively. The solid lines are the results from HNC/MSA.

TABLE 2: ζ-potential of a DNA-sized Rod (see Table 1) Immersed into a 0.49 M Electrolyte of 2:2 Salt as a Function of Its Manning Parameter ξ[a]

ξ	ζ_{LPB}	ζ_{PB}	ζ_{HNC}	ζ_{MD}
0	0	0	0	0
1.05	10.52	10.28	6.262	9.116
2.1	21.04	19.48	10.99	14.62
4.2	42.09	33.32	14.27	16.25
6.3	63.13	42.96	11.08	13.80
8.4	84.17	50.16	3.771	9.263
10.5	105.2	56.03	−6.219	3.675

[a] The four predictions are from linear PB theory, PB theory, HNC theory, and MD simulation. The error in the MD simulation is estimated to be of the order of 2%. Figure 5 visualizes the data. The values for the four predictions are stated in millivolts.

which can be identified with the ζ-potential of electrophoresis and which is important in the computation of electrophoretic mobilities.[31,46] In the PB theory for a charged rod immersed into an ionic solution, and its linearized version, ζ depends monotonically on ξ.[18] However, Figure 2 shows that $\psi(r)$ can become negative in the presence of overcharging,. This calls the monotonic relation between ζ and ξ into question. Table 2 summarizes various predictions for the ζ-potential as a function of the Manning parameter together with results from the MD simulations. A graphical illustration is given in Figure 5. Indeed, ζ is found to first increase with ξ, but from a certain value on it decreases and finally even becomes negative. Note that this would reverse the drift direction in electrophoresis measurements, as first predicted by Gonzales-Tovar et al.[18] and recently demonstrated, for spherical macroions, by Lozada-Cassou et al.[31] Although nonlinear and linearized PB theories coincide with the data and with each other for small Manning parameters,

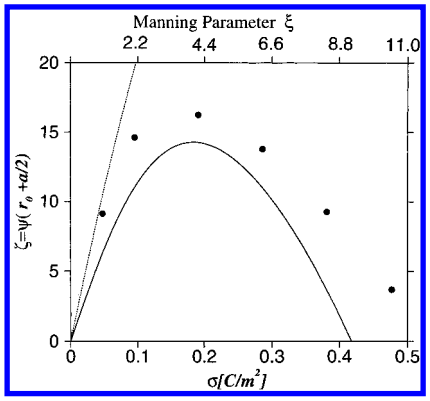

Figure 5. Zeta potential $\zeta \equiv \psi(r_0 + a/2)$ as a function of surface charge density σ, for a cylinder immersed in a 0.49 M 2:2 electrolyte. The model parameters are given in Table 1. The dotted line is the prediction of PB theory, the dots are the MD results, and the solid line is the results from HNC/MSA calculations.

they completely fail to predict the back-bending, which already sets in at comparatively small values of ξ. The HNC/MSA theory captures this effect, but it underestimates the value of the potential. However, comparisons for the ζ-potential, as a function of σ, between HNC/MSA and MC simulations for planar and spherical hard, charged macroions, immersed into a RPM electrolyte, have been made previously.[25,43,47] For these two geometries, for 1:1 and 2:2electrolytes, at about 0.5 M, as in Figure 5, the HNC/MSA-MC agreement is excellent. The disagreement seen in Figure 5 can be related to the different short-range potentials used in our MD and HNC/MSA calculations, which does not give for the MD a sharply defined ion-cylinder contact. This is important, because the ζ-potential is evaluated exactly there. For planar and spherical macroions, PB ζ vs charge curves are also above the HNC/MSA and MC curves, which is consistent with our present observations.

For a given rod charge and diameter, for any electrolyte solution parameters, a higher ζ-potential always implies a smaller ionic size.[18] A soft-repulsive short-range potential, as in our MD calculations, allows the counterions to get closer to the rod. This produces a higher ζ-potential in the MD simulation when compared with the HNC/MSA results. In the PB theory, the neglect of the ionic-size correlations allows a higher density of counterions next to the rod, which in turn can never lead to overcharging.

In all cases, the HNC/MSA qualitative agreement with MD is very good. The success of HNC/MSA theory indicates that local ion-size correlations are responsible for both phenomena. As Lozada-Cassou and Jiménez-Ángeles conclude in ref 48, overcharging increases with an increase of the system excluded volume, i.e., higher ionic size and/or concentration. If size correlations are not considered (as in PB theory) or are negligible, overcharging does not occur, even for divalent ions. On the other hand, overcharging can occur in a high excluded volume system even for monovalent ions. To illustrate this fact we have simulated two systems for which the distance of closest approach to the charged rod is 9.98 Å in both cases, hence DNA-like. The first rod system has a charge parameter of $\xi = 4.2$ ($\sigma = 0.240$ C/m^2) and is immersed in a 1.0 M 1:1 electrolyte solution with ions of diameter $a = 7.4$ Å. The second rod system has an even higher charge parameter of $\xi = 10.5$ ($\sigma = 0.40$ C/m^2) and is immersed in a 0.5 M 2:2 electrolyte, but, this time, the diameter is only $a = 1.0$ Å. The results are shown in Figure 6, where the charge distribution function is plotted. Contrary to the general believe, the system with the large monovalent ions shows overcharging, both in the HNC/MSA and the MD

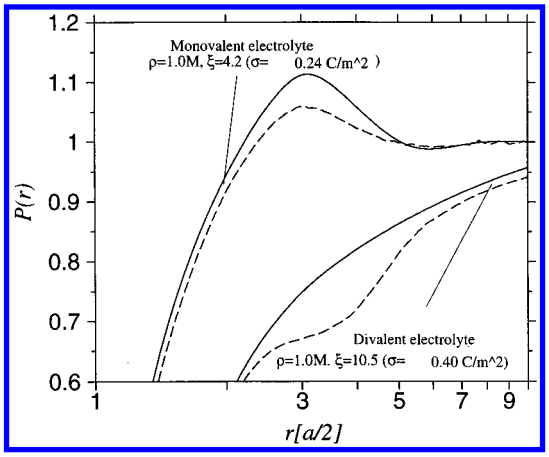

Figure 6. Charge distribution function from HNC/MSA (solid lines) and MD (dotted lines) for a RPM electrolyte next to a charged cylinder to which the ions have a distance of closest approach of 9.98 Å. The distance r is measured with respect to the cylinder surface in units of the ionic radius. In this plot a comparison between a low and a high excluded volume system is presented. The system where overcharging occurs corresponds to a monovalent electrolyte with $\rho = 1.0$ M, $\xi = 4.2$ ($\sigma = 0.240$ C/m^2), and large ions ($a = 7.4$ Å). The system where overcharging is not observed corresponds to a divalent electrolyte with $\rho = 0.5$ M, $\xi = 10.5$ ($\sigma = 0.40$ C/m^2), and small ions ($a = 1.0$ Å).

results, and the location of the peaks coincide, whereas we see small differences in the height. Further, strikingly, the system with small divalent ions shows no sign of overcharging, although the charge parameter for this system is even higher. The shoulder in the distribution of the MD simulation indicates that the second ionic layer is almost neutral. A possible explanation is that the small ions have an energy of attraction of almost 30 k_BT, hence the salt is actually present in the form of little overall neutral salt clusters. This is supported by visual inspection of the MD configurations. These mostly neutral clusters are polarizable and hence tend to accumulate in the large field gradient surrounding the rod. The free counterions left can come only from the rods charge and can in no way lead to an overcharging. A key prerequisite for this scenario is that the interaction energy between ions exceeds the interaction between ions and the rod. Also consistent, the HNC/MSA calculation as well shows the vanishing of the overcharging.

Finally, one might ask how the effect of overcharging depends on salt concentration. Obviously there cannot be any overcharging in the absence of salt, because then even a complete "condensation" of all ions would merely neutralize the rod. However, it is not clear from the beginning whether an addition of just *some* salt will immediately lead to overcharging. Figure 7 shows HNC/MSA and MD distribution functions $P(r)$ and mean electrostatic potentials $\psi(r)$ for a DNA-sized and charged rod, immersed into a 2:2 electrolyte, for varying salt concentrations. The phenomenon of overcharging is indeed observed, but only at sufficiently high salt concentrations. These results are consistent with the fact that higher electrolyte concentration increases the excluded volume, thus increases overcharging.[48] Therefore, as proposed in ref 48, higher excluded volume implies higher overcharging. This may also be illustrated by defining r_1 to be the radius at which overcharging sets in, i.e.,

$$r_1 = \min\{r: P(r) = 1\} \tag{24}$$

Figure 8 illustrates the measured r_1 together with a HNC prediction as a function of salt concentration ρ_s. Clearly, r_1 must increase with decreasing ρ_s, because overcharging is reduced, and consequently the size of the charge-compensating layer must

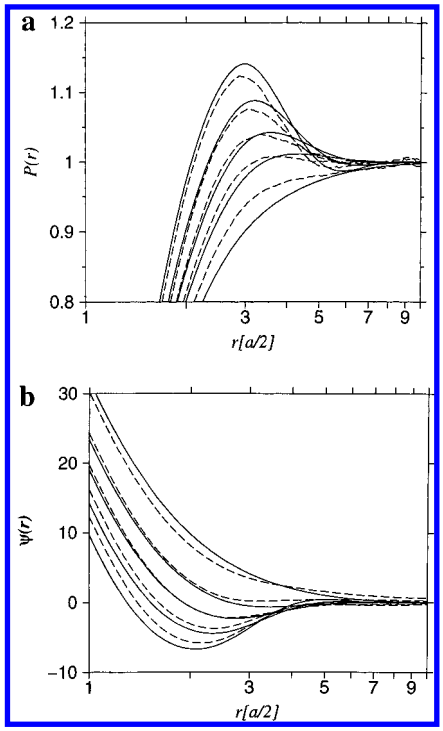

Figure 7. Charge distribution function $P(r)$ (a) and mean electrostatic potential $\psi(r)$ (b) results for the system from Table 1 with Manning parameter $\xi = 4.2$. The distance r is measured with respect to the cylinder surface in units of the ionic radius. The line styles have the same meaning as in Figure 2. The curves correspond to different salt concentrations, $\rho_s = 0.12$, 0.24, 0.34, 0.49, 0.68 M. In the charge distribution function the salt content increases from bottom to top, in the mean electrostatic potential it increases from top to bottom.

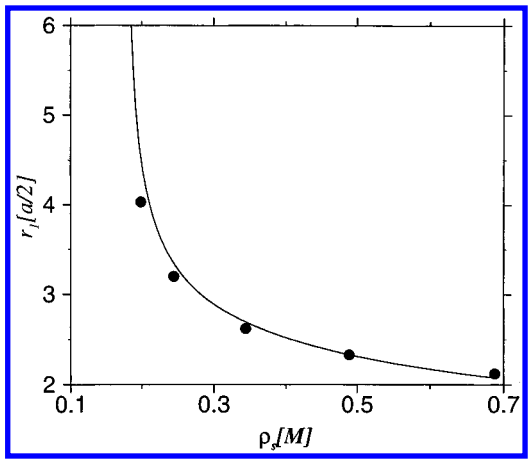

Figure 8. Radius r_1 from eq 24 at which overcharging sets in, for a DNA-sized and -charged cylinder ($r_0 = 7.86$ Å and $\sigma = 0.190$ C/m^2), as a function of salt concentration ρ_s. The distance r_1 is measured with respect to the cylinder surface in units of the ionic radius. The dots are the results of MD simulations, and the solid line is the prediction of HNC/MSA.

increase. In fact, HNC theory predicts that $r_1(\rho_s)$ diverges at some *finite* density $\rho_s^\infty \approx 0.18$ mol/L corresponding to a salt Debye length of 3.59 Å, or roughly 200 salt molecules within the simulation box. For the lower concentrations, the simulated r_1 values lie below the HNC prediction, but this is not a feature that is generally expected. Figure 7 shows that the stronger overcharging in HNC theory should generally lead to a value of r_1 smaller than in the simulation. But with decreasing density the finite radius of the simulation cell becomes relevant. Indeed, zero-salt distribution functions reach the value 1 at the cell boundary, and not at infinity. A reduction of the amount of

added salt at fixed cell radius must necessarily lead to values of r_1 smaller than the HNC prediction for the bulk, because within a finite cell r_1 cannot diverge. On the other hand, for technical reasons, the MD cell radius cannot be increased indefinitely. In any case, our MD results have not been able to unambiguously detect overcharging at densities equal to or lower than 0.2 M, which is in excellent agreement with the HNC/MSA prediction for the minimum amount of salt needed to induce overcharging. Figures 7 and 8 clearly show that excluded volume effects determine the occurrence of overcharging, as some of us have proposed.[48]

V. Conclusion

Theoretical and numerical studies of stiff linear polyelectrolytes, immersed into a 2:2 RPM electrolyte have been presented. The qualitative agreement between the MD and HNC/MSA results is excellent. For the DNA parameters, in particular, there is also a very good quantitative agreement. We argued that the better agreement in the planar and spherical case reported in refs 25, 43, and 47 is probably due to an implementation of the short-range interactions that is identical with the theoretical model and not merely very close. At low salt concentrations the difference between a finite cell used in simulations and the $R = \infty$ system used in the HNC/MSA calculations becomes important. Also, the macroion and ions electrical fields are much less screened and, hence, the charge correlations become more important.[2] Both these points are responsible for the disagreement between theory and simulations at low salt. Although the former can in principle be resolved by increasing the size of the simulation cell, the latter can be addressed by the three-point extension HNC/MSA theory,[17,40] which gives a better account of these correlations.[48]

In the past the HNC/MSA theory for an electrolyte next to a charged rod has been derived[17] and applied[18] to simple DNA models. In this article we have shown this theory to be qualitatively correct. In particular, for DNA parameters the quantitative agreement is excellent. To the best of our knowledge, in Gonzales-Tovar et al.[18] overcharging has first been predicted theoretically. It was pointed out that this should entail an electrophoresis mobility reversal. In the PB theory the ζ-potential as a function of the cylinder charge density is a monotonic function, whereas in the HNC/MSA theory it is not. In this article we have shown the HNC/MSA prediction to be in agreement with MD calculations. This nonmonotonic behavior of the ζ-potential has important implications in electrophoresis calculations. The standard electrophoresis theory[21,22] is based on the PB prediction for ζ and, hence, important differences should be found if the HNC/MSA theory is applied to the electrophoresis problem.

Recently, Lozada-Cassou et al.[31] extended the electrophoresis theory to include ionic size effects, through the HNC/MSA theory. It was applied to spherical macroions. A mobility reversal and a very nonlinear behavior of the mobility, as a function of the ζ-potential, were predicted. These predictions were found to be in agreement with experimental results. Contrary to the standard electrophoresis theory, the mobility was shown to be nonuniversal. This is due precisely to the nonmonotonic behavior of the ζ-potential. The HNC/MSA and MC simulations for spherical and planar macroions do not show a maximum in $\zeta(\sigma)$ as pronounced as that reported here for the cylindrical geometry. Therefore, we believe that our HNC/MSA and MD results are particularly relevant.

In view of the qualitative agreement between HNC/MSA and MD and the quantitative and qualitative disagreement of these with PB theory, we conclude that for concentrated and divalent electrolytes, influenced by charged polyelectrolytes, the size correlations must be taken properly into account to describe the cylindrical double layer. Our MD results clearly indicate that overcharging strongly depends on the system excluded volume, as proposed by some of us.[48] While maximum overcharging does not seem to have a limit, the minimum conditions to have overcharging depend on many different ways in which ionic charge, size and concentration, and surface charge density participate in a system, as we showed in Figures 2, 6, and 7.

Acknowledgment. C.H. and M.L.C. thank W. Gelbart and The Institute for Theoretical Physics, University of California at Santa Barbara, where this project was started, for their hospitality. M.L.C. thanks C. Holm and K. Kremer for their hospitality at Mainz. F.J.A. and M.L.C. gratefully acknowledge the financial support of INDUSTRIAS NEGROMEX. C.H. and M.D. acknowledge a large computer time grant hkf06 from NIC Jülich and financial support by the German Science foundation.

References and Notes

(1) Barrat, J. L.; Joanny, J. F. *Adv. Chem. Phys.* **1996,** *94*, 1.
(2) Lozada-Cassou, M.; Díaz-Herrera, E. *J. Chem. Phys.* **1990,** *93*, 1386.
(3) Sánchez, J. E.; Lozada-Cassou, M. *Chem. Phys. Lett.* **1992,** *190*, 202.
(4) Jiménez-Ángeles, F.; Messina, R.; Holm, C.; Lozada-Cassou, M., in preparation.
(5) Alfrey, T.; Berg, P.; Morawetz, H. J. *J. Polym. Sci.* **1951,** *7*, 543.
(6) Fuoss, R. M.; Katchalsky, A.; Lifson, S. *Proc. Natl. Acad. Sci. U.S.A.* **1951,** *37*, 579.
(7) Manning, G. *J. Chem. Phys.* **1969,** *51*, 924.
(8) Oosawa, F. *Polyelectrolytes*; Marcel Dekker: New York, 1971.
(9) Deserno, M.; Holm, C.; May, S. *Macromolecules* **2000,** *33*, 199.
(10) Bloomfield, V. *Biopolymers* **1991,** *31*, 1471.
(11) Valleau, J. P.; Ivkov, R.; Torrie, G. M. *J. Chem. Phys.* **1991,** *95*, 520.
(12) Nilsson, L. G.; Guldbrand, L.; Nordenskiöld, L. *Mol. Phys.* **1991,** *72*, 177.
(13) Lyubartsev, A. P.; Tang, J. X.; Janmey, P. A.; Nordenskiöld, L. *Phys. Rev. Lett.* **1998,** *81*, 5465.
(14) Lozada-Cassou, M.; Henderson, D. *Chem. Phys. Lett.* **1986,** *127*, 392.
(15) Kjellander, R.; Marcelja, S. *J. Phys. Chem.* **1986,** *90*, 1230.
(16) Lozada-Cassou, M.; Díaz-Herrera, E. *J. Chem. Phys.* **1990,** *92*, 1194.
(17) Lozada-Cassou, M. *J. Phys. Chem.* **1983,** *87*, 3279.
(18) Gonzales-Tovar, E.; Lozada-Cassou, M.; Henderson, D. *J. Chem. Phys.* **1985,** *83*, 361.
(19) Greberg, H.; Kjellander, R. *J. Chem. Phys.* **1998,** *108*, 2940.
(20) Hidalgo-Álvarez, R.; Martín, A.; Fernández, A.; Bastos, D.; Martínez, F.; de las Nieves, F. J. *Adv. Colloid Interface Sci.* **1996,** *67*, 1; review article.
(21) Wiersema, P. H.; Leob, A. L.; Overbeek, J. Th. G. *J. Colloid Interface Sci.* **1966,** *22*, 78.
(22) O'Brien, R. W.; White, L. R. *J. Chem. Soc., Faraday Trans. 2* **1978,** *74*, 1607.
(23) Torrie, G. M.; Valleau, J. P. *J. Chem. Phys.* **1980,** *73*, 5807.
(24) Vlachy, V.; Haymet, A. O. J. *J. Chem. Phys.* **1986,** *84*, 5874.
(25) Degrève, L.; Lozada-Cassou, M.; Sáncez, E.; González-Tovar, E. *J. Chem. Phys.* **1993,** *98*, 8905.
(26) Degrève, L.; Lozada-Cassou, M. *Mol. Phys.* **1995,** *86*, 759.
(27) Strauss, U. P.; Gershfeld, N. L.; Spiera, H. *J. Am. Chem. Soc.* **1954,** *76*, 5909.
(28) Elimelech, M.; O'Melia, C. R. *Colloids Surf.* **1990,** *44*, 165.
(29) Wang, Y.; Kimura, K.; Huang, Q.; Dubin, P. L. *Macromolecules* **1999,** *32*, 7128.
(30) Huang, Q. R.; Dubin, P. L.; Moorefield, C. N.; Newkome, G. R. *J. Phys. Chem. B* **2000,** *104*, 898.
(31) Lozada-Cassou, M.; González-Tovar, E.; Olivares, W. *Phys. Rev. E* **1999,** *60*, R17.
(32) Shklovskii, B. I. *Phys. Rev. E* **1999,** *60*, 5802.
(33) Nguyen, T. T.; Yu Grosberg, A.; Shklovskii, B. I. *Phys. Rev. Lett.* **2000,** *85*, 1568.

(34) Frenkel, D.; Smit, B. *Understanding Molecular Simulation*; Academic Press: San Diego, 1996.
(35) Deserno, M.; Holm, C. *J. Chem. Phys.* **1998,** *109*, 7678.
(36) Deserno, M.; Holm, C. *J. Chem. Phys.* **1998,** *109*, 7694.
(37) Hockney, R. W.; Eastwood, J. W. *Computer Simulation Using Particles*; Hilger: Bristol, U.K., 1988.
(38) Grest, G. S.; Kremer, K. *Phys. Rev. A* **1986**, *33*, 3628.
(39) Henderson, D. In *Fundamentals of inhomogeneous fluids* Marcel Dekker: Edited by D. Henderson 1992; Chapter 4.
(40) Lozada-Cassou, M. In *Fundamentals of Inhomogeneous Fluids*; Henderson, D., Ed.; Marcel Dekker: New York, 1992; Chapter 8.
(41) Lozada-Cassou, M.; Olivares, W.; Sulbarán, B. *Phys. Rev. E* **1996,** *53*, 522.
(42) Yu, J.; Degrève, L.; Lozada-Cassou, M. *Phys. Rev. Lett.* **1997,** *79*, 3656.
(43) Degrève, L.; Lozada-Cassou, M. *Phys. Rev. E* **1998,** *57*, 2978.
(44) Lozada-Cassou, M. *J. Chem. Phys.* **1981,** *75*, 1412; **1982,** *77*, 5258.
(45) Mier y Terán, L.; Díaz-Herrera, E.; Lozada-Cassou, M.; Saavedra-Barrera, R. *J. Comput. Phys.* **1989,** *84*, 326.
(46) Hunter, R. J. *Foundations of Colloid Science;* Oxford Science Publications, Clarendon Press: Oxford, 1987; Vol. 1.
(47) Lozada-Cassou, M.; Saavedra-Barrera, R.; Henderson, D. *J. Chem. Phys.* **1982,** *77*, 5150; Lozada-Cassou, M.; Henderson, D. *J. Phys. Chem.* **1983**, *87*, 2821.
(48) Lozada-Cassou, M.; Jiménez-Ángeles, F., in press. *(cond-matt/0105043)*